BAMS Article

The Advanced Very High Resolution Radiometer

Contributing to Earth Observations for over 40 Years

S. Kalluri, C. Cao, A. Heidinger, A. Ignatov, J. Key, and T. Smith

ABSTRACT: The Advanced Very High Resolution Radiometers (AVHRR), which have been flying on National Oceanic and Atmospheric Administration's (NOAA) polar-orbiting weather satellites since 1978, provide the longest global record of Earth observations from a visible–infrared imager. Experience gained through AVHRRs has been integral to the development of the new-generation sensors such as the Moderate Resolution Imaging Spectroradiometer (MODIS), the Visible Infrared Imaging Radiometer Suite (VIIRS), and associated data processing algorithms in the United States, as well as a similar class of sensor by space agencies around the world. Over four decades of data have been vital for studying Earth and its change. The *MetOp-C* satellite that was successfully launched in 2018 carries the last AVHRR. This article reviews the contributions of AVHRR in building a continuous global data record over the last 40 years on the occasion of its last launch.

https://doi.org/10.1175/BAMS-D-20-0088.1
Corresponding author: S. Kalluri, satya.kalluri@noaa.gov
In final form 17 August 2020

AFFILIATIONS: Kalluri, Cao, Ignatov, and Smith—NOAA/NESDIS/STAR, College Park, Maryland; **Heidinger**—NOAA/NESDIS, Madison, Wisconsin; **Key**—NOAA/NESDIS/STAR, Madison, Wisconsin

The Television Infrared Observation Satellite (TIROS-N) launched in 1978 carried the first Advanced Very High Resolution Radiometer (AVHRR), a prototype digital imaging system designed to capture visible and infrared images of Earth for meteorology. Since then, AVHRRs have been flown continuously on NOAA's Polar Operational Environmental Satellites (POES) for over 40 years. In 1998, NOAA and the European Organisation for the Exploitation of Meteorological Satellites (EUMETSAT) signed the Initial Joint Polar Satellite System (IJPS) agreement. Under this agreement, EUMETSAT launched and operated the Meteorological Operational satellite (MetOp) in midmorning orbit while NOAA operated its POES in the midafternoon orbit. Both POES and MetOp satellites carried the AVHRR. The midmorning MetOp satellite has an equatorial crossing time of ascending node around 0930 local time and the midafternoon POES has an equatorial crossing time around 1430 local time when they are declared operational. The third and last first generation, *MetOp-C* was successfully launched on 7 November 2018 and carries the last planned AVHRR.

There have been three generations of AVHRR. The first generation, AVHRR/1, flew on TIROS-N and *NOAA-6*/*-8*/*-10*, and was a four-channel imaging radiometer. The next model (AVHRR/2) was a five-channel imager. The third generation, AVHRR/3, was flown on the NOAA-KLMN series beginning in 1998 and on the *MetOp-A*/*-B*/*-C* satellites beginning in 2006. It has six channels, although only five channels could be transmitted at any given time (Table 1) (Kidwell 1995). A timeline of NOAA and EUMETSAT satellites that carried the AVHRR is shown in Fig. 1.

AVHRR has provided an invaluable >40-yr global record for monitoring and understanding land (including biogeophysical processes and land use, cover, and dynamics), atmosphere (cloud and aerosols), ocean (sea surface temperature, currents, fronts, and water turbidity), and cryosphere (snow and ice cover), in support of both operational meteorology and oceanography, and global change studies. Highlights of AVHRR's contributions were presented by Kalluri et al. (2019) at the International Geoscience and Remote Sensing Symposium and this article provides a more comprehensive review. While the emphasis of this paper is on AVHRR's contributions to building the longest satellite-based global climate data record, there are several operational meteorological applications that rely on AVHRR as well. For example, the sea surface temperature (SST) (Ignatov et al. 2016) is used by NOAA's CoastWatch program (NOAA 2020), Arctic composite imagery are used for visual interpretation and situational awareness, atmospheric motion vectors over polar regions (Velden et al. 2005) are used in numerical weather prediction (NWP) models, global vegetation indices are used for drought monitoring (Van Hoolst et al. 2016), and snow- and ice-cover analysis are used for near-real-time monitoring of polar regions (Key et al. 2016).

AVHRR design and lessons learned

Initially designed in the late 1970s to observe global cloud coverage, land characteristics, sea surface temperature, ice, and snow cover, the AVHRR is well known for its simple and

Table 1. Spectral bands and their wavelengths (μm) of AVHRR flown on different NOAA and MetOp satellites.

	Satellites		
Band No.	TIROS-N, *NOAA-6*/*-8*/*-10*	*NOAA-7*/*-9*/*-11*/*-12*/*-13*/*-14*	*NOAA-15*/*-16*/*-17*/*-18*/*-19 MetOp-A*/*-B*/*-C*
1	0.58–0.68	0.58–0.68	0.58–0.68
2	0.725–1.10	0.725–1.10	0.725–1.10
3A	—	—	1.58–1.64
3B	3.55–3.93	3.55–3.93	3.55–3.93
4	10.50–11.50	10.3–11.3	10.3–11.3
5	Band 4 repeated	11.5–12.5	11.5–12.5

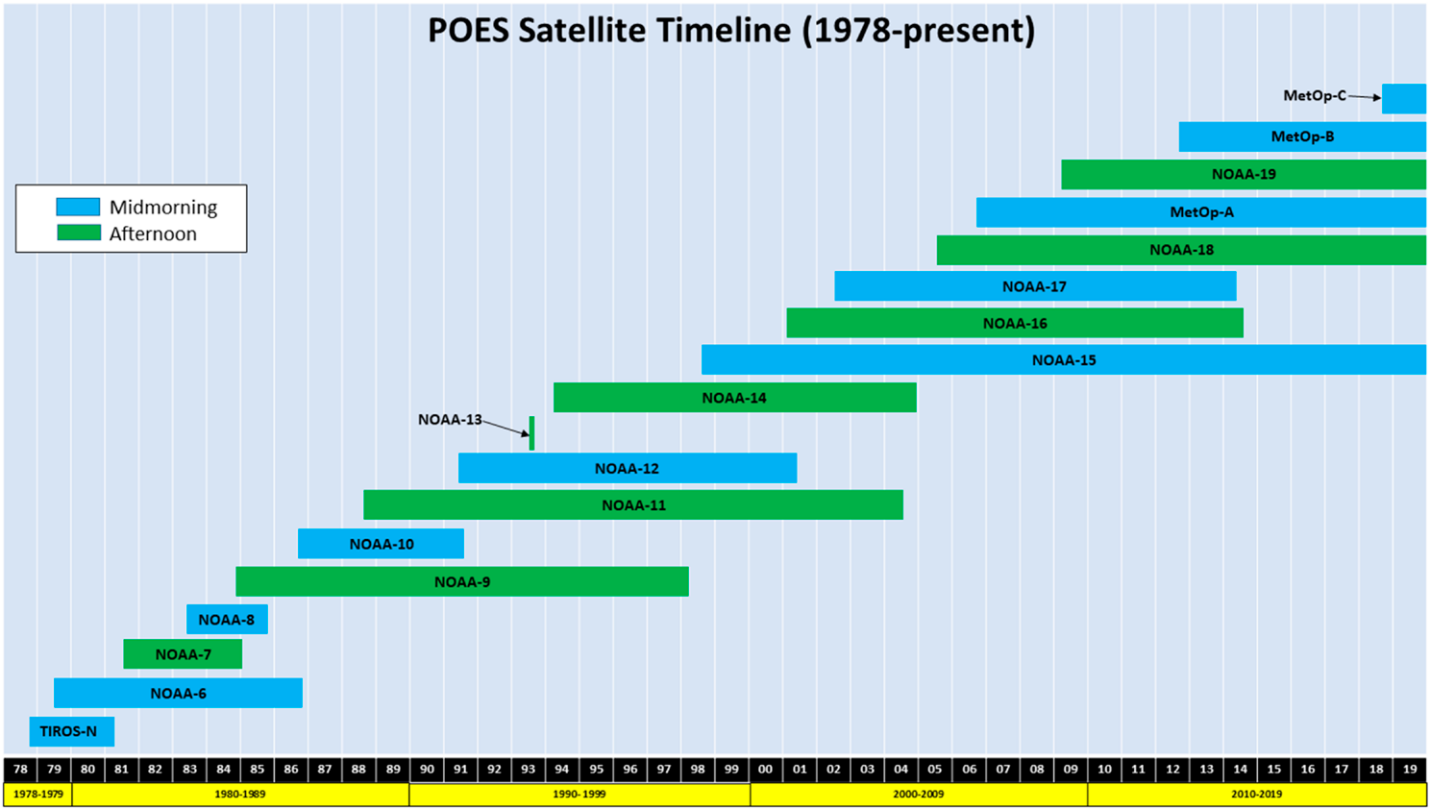

Fig. 1. A timeline of NOAA and MetOp missions that carried the AVHRR.

robust design as a cross-track line-scanning radiometer. The incident Earth radiation is collected with a traditional 45° scan mirror in the fore optics and then split into channels using a combination of beam splitters and filters. A single detector is used for each channel which greatly reduces the complexities and also leads to great consistency in the spectral response across scans. The thermal infrared detectors are passively cooled down to ~105 K, while the visible–near-infrared bands operate at ambient temperature. The incident radiance on the detector generates a voltage that is amplified and in turn converted to a 10-bit digital count for downlink. The AVHRR band spectral responses are fairly broad by modern standards, which was necessary at the time in order to collect enough photons to achieve the signal to noise ratio desired. The simplicity in the AVHRR design contributed to its great success in the last four decades, which has become one of the most reliable instruments in the history of NOAA satellites. The reader is referred to Cracknell (1997) for a detailed description of the sensor.

The visible (and near-infrared) bands (also known as reflective solar bands) have no onboard calibration and therefore rely on several vicarious calibration methods to account for the sensor responsivity degradation over time, including a stable Libyan desert site, deep convective clouds (DCC), and simultaneous nadir overpass (SNO) with radiometers on other satellites (Rao and Chen 1999; Heidinger et al. 2002). The calibration accuracy of the reflective solar bands is estimated to be typically better than 5%, although it highly depends on the methodology and algorithm used (Cao et al. 2008). The broad channel spectral response in each channel also presents challenges for applications especially due to water vapor absorption in the 0.86-μm band. The AVHRR geolocation accuracy is typically better than 1 km, which is moderate by modern standards. Although AVHRR was never intended to be a climate-monitoring instrument, various techniques to intercalibrate the many radiometers launched since 1978 enabled the development of long time series suitable to the study of global change. To address the calibration inconsistencies in the operational AVHRR datasets, reprocessing efforts have been made to improve the long-term time series of the AVHRR data record.

The infrared bands (also known as thermal emissive bands) of AVHRR are calibrated on board using a full aperture blackbody and views of the deep space for each scan. The blackbody temperature floats around ~290 K with the instrument with an orbital variation about 2 K. This linear calibration using two calibration points is augmented by a nonlinear calibration equation, for which the quadratic term is derived in prelaunch testing. The dynamic range of the AVHRR infrared channels is 180–335 K. While the low end of the temperature range allows observations of clouds, ice and snow, and polar regions, the infrared bands may saturate when observing hot targets such as fires and desert. Despite the simple design and limitations, studies have shown that the thermal infrared bands of AVHRR calibration accuracy is within 0.5 K compared to the Infrared Atmospheric Sounding Interferometer (IASI) and the Moderate Resolution Imaging Spectroradiometer (MODIS), with slight orbital variations due to orbital thermal dynamics (Cao et al. 2004; Wang and Cao 2008). Since all legacy NOAA satellites drift in orbit over time, the calibration biases can be mixed with diurnal variations of the observations, such as sea surface temperatures, as well as solar contamination issues on the AVHRR instrument due to its wide-open fore optics. Thus, even though all the AVHRRs in history had similar design, their ability to make consistent Earth observations at the same local time degraded during the life of each mission. Several "Pathfinder" reprocessing efforts attempted to intercalibrate and consistently reprocess data from all AVHRRs, to minimize spurious signals due to calibration and changes in observation time of day (James and Kalluri 1994).

The advantages and disadvantages of the AVHRR design have been studied by many researchers, and the lessons learned contributed greatly to the new generation of imaging radiometers with improved performance in radiometric, spatial, and spectral characteristics. A large number of bands have been added to follow-on instruments such as MODIS (Salomonson et al. 1989), the Visible Infrared Imaging Radiometer Suite (VIIRS) (Cao et al. 2014), and METImage (Phillips et al. 2016) with much narrower spectral bandwidth, and with multiple detectors per scan. Onboard calibration devices have been added, such as a solar diffuser (SD) and solar diffuser stability monitors (SDSM) to improve the calibration accuracy of the reflective solar bands. Geospatial performance has also been improved significantly for modern instruments. For example, a rotating telescope has been introduced on VIIRS to enhance the off-nadir performance of the radiometer and greatly reduce stray light contamination. Modern GPS systems on board the satellite also enable sub-pixel-level geolocation accuracy. The orbital drift problem has also been addressed with the launch of *MetOp-A* and *Suomi NPP* satellites, for the morning and afternoon satellites, respectively, where the spacecraft orbit is actively controlled. All these improvements greatly facilitate the use of the new-generation Earth imaging satellite data, with rapidly expanding applications. Nevertheless, the four decades of historical data records collected by AVHRR are irreplaceable for long-term time series studies.

Figure 2 shows the spectral response functions of AVHRR's two solar bands, compared to the seven bands of MODIS and VIIRS

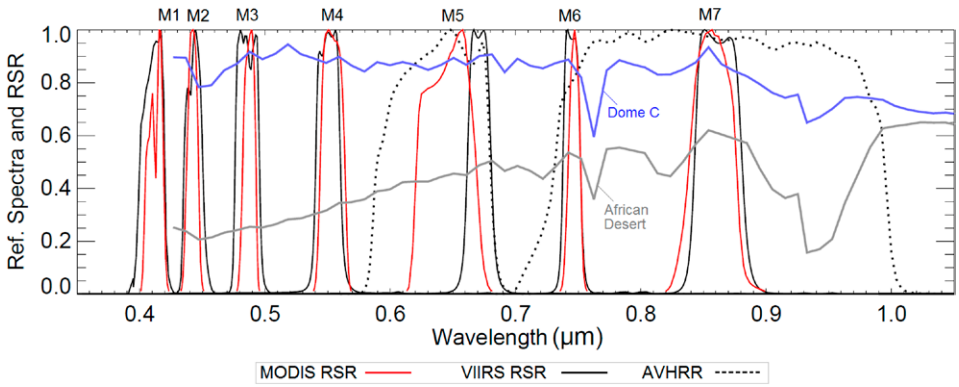

Fig. 2. Relative spectral response function (RSR) of solar reflective bands on AVHRR, VIIRS, and MODIS in the 0.4–1.0-μm spectral region. Sample spectra of Libyan desert and Dome C snow field in Antarctica are also shown as these sites are used as vicarious calibration targets.

covering the 0.4–1.0-μm spectral region. The third-generation AVHRRs has a channel 3a centered at 1.6 μm (half duty cycle), compared to the additional four bands in VIIRS from 1 to 2.5 μm. The broad spectral response of AVHRR causes uncertainties in both spectral and radiometric accuracy and stability. The absolute radiometric calibration also suffers from the lack of traceability and standards. When we compare VIIRS with AVHRR equivalent channels over the Libyan desert (Fig. 3), AVHRR channel 1 on *NOAA-19* (which was launched in a similar orbit as *Suomi NPP* VIIRS) is relatively stable based on a 2-yr assessment since *Suomi NPP* launch in 2011. However, AVHRR reflectances are biased too low by ~8.6% ± 0.9% after accounting for the spectral band adjustment factor (SBAF), due to the lack of traceability of radiometric standards (Cao et al. 2008). In contrast, AVHRR channel 2 on *NOAA-19* calibration oscillates seasonally based on the desert calibration, due to water vapor absorption in the AVHRR spectral response for this channel which is propagated into the desert-based calibration. The bias is on the order of 17.1% ± 2% after accounting for the SBAF although it is more difficult to provide a very accurate assessment due to the large spectral differences for this AVHRR channel compared to the equivalent VIIRS channel (M7). In addition, AVHRR channel 1 appears to have a residual degradation after calibrated using the desert target, shown as a long-term residual degradation trend of ~1.2%.

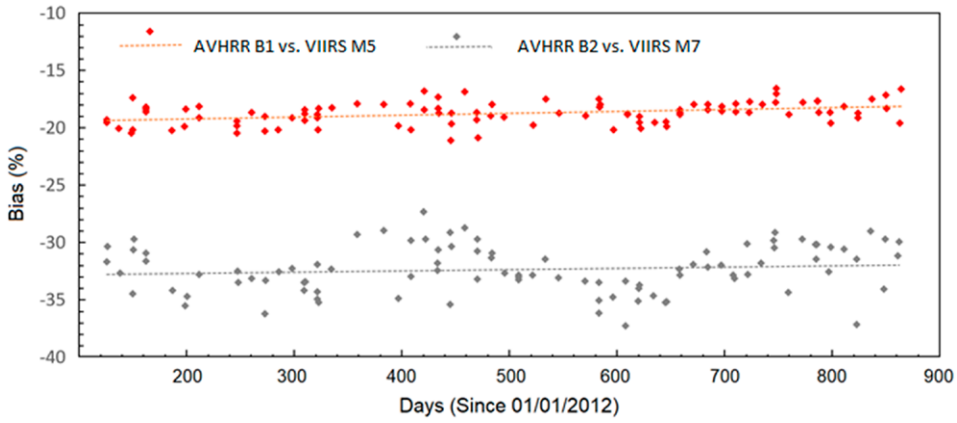

Fig. 3. Top-of-atmosphere (TOA) reflectance bias between VIIRS and AVHRR over the Libyan desert with near-simultaneous nadir observations for channels 1 (red) and 2 (gray) before SBAF adjustment [Bias = (AVHRR − VIIRS)/VIIRS × 100%]. Dashed lines show residual degradation trend for AVHRR channels.

Because of differences in spectral band characteristics and calibration approaches among different imagers, there will be differences in observed parameters such as the normalized difference vegetation index (NDVI) as seen in Fig. 4. While there is a good agreement among

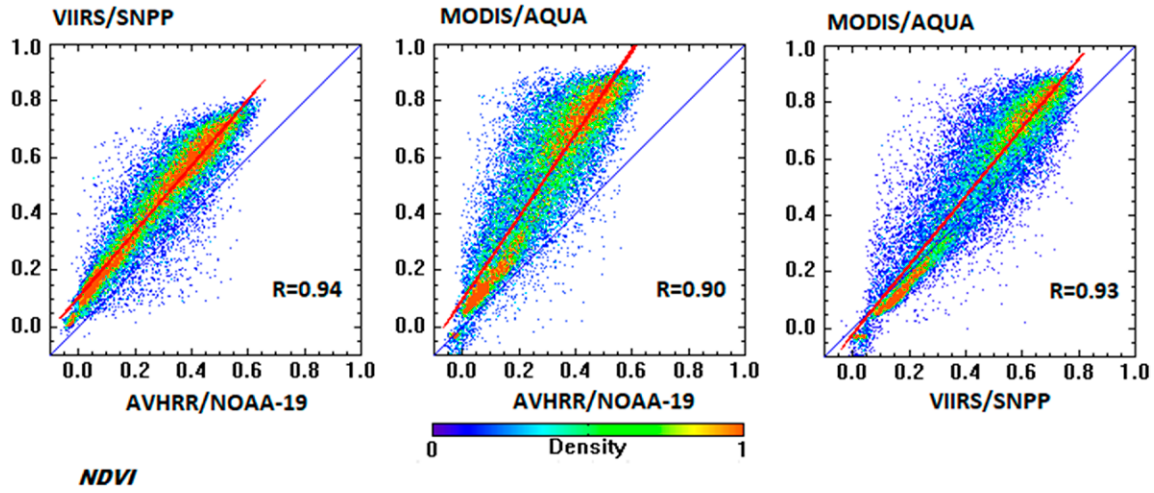

Fig. 4. Correlation of mean NDVI (40°N–40°S) measured by AVHRR, VIIRS, and MODIS during July 2012. While there is good correlation among the measurements made by different sensors, there are obvious biases between them (courtesy: Felix Kogan, NOAA/NESDIS/STAR).

NDVIs derived from AVHRR, MODIS and VIIRS, there are nevertheless systematic biases between them. Such differences can lead to inconsistencies in building long-term climate data records, which need to be resolved through satellite intercalibrations (Trishchenko 2009; Zhang et al. 2017)

AVHRR contributions to terrestrial studies

Schneider et al. (1981) first demonstrated the usefulness of AVHRR data for successfully discriminating and monitoring terrain features using *NOAA-6* data. This study was based on previous knowledge gained through analysis of multispectral sensor data on board the Landsat satellites. Discrimination between lake ice, snow cover, inland water bodies, and especially the use of vegetation indices and their sensitivity to crop condition and chlorophyll content over different terrain types was demonstrated. The red (AVHRR band 1) and near-IR (AVHRR band 2) spectral bands offer significant information about vegetation because of contrasting spectral signatures in these wavelengths, and NDVI [NDVI = (Band 2 − Band 1)/(Band 2 + Band 1)] is one of the most widely used band combinations from AVHRR (Holben 1986). Temporal composites of NDVI have been extensively used for a wide variety of applications, such as modeling biogeochemical cycles, land-use–land-cover change, drought monitoring, vector-borne disease modeling, hydrological modeling, and climate change. Although NOAA has been producing vegetation indices operationally since 1982 at global scales, the techniques to improve the indices have gradually evolved and improved over time (Townshend 1994).

Based on earlier pioneering work using NDVI to study vegetation dynamics at continental scale using global area coverage (GAC) data (Justice et al. 1985), agencies such as U.S. Agency for International Development (USAID) started using it for drought monitoring in Africa since 1988 (Brown and Brickley 2012). NDVI is now an integral part of the Famine and Early Warning Systems (FEWS) (Hutchinson 1991). Various combinations of NDVI and temperature are used for assessing vegetation health (Kogan 1997) (Fig. 5). Local area coverage (LAC) data collected by several countries around the world have become a vital tool for local and regional-level crop condition reports such as the U.S. Drought Monitor. Albedo and surface temperatures from AVHRR are used as inputs to model energy balance and sensible and latent heat fluxes on ground, which are indicators of soil moisture and vegetation condition. Empirical and theoretical models, linking vegetation indices with vegetation biophysical parameters, such as leaf-area index, the fraction of photosynthetically active radiation absorbed, also emerged in the 1980s, which allowed scientists to model processes such as net primary production and carbon fluxes from vegetation (Tucker and Sellers 1986).

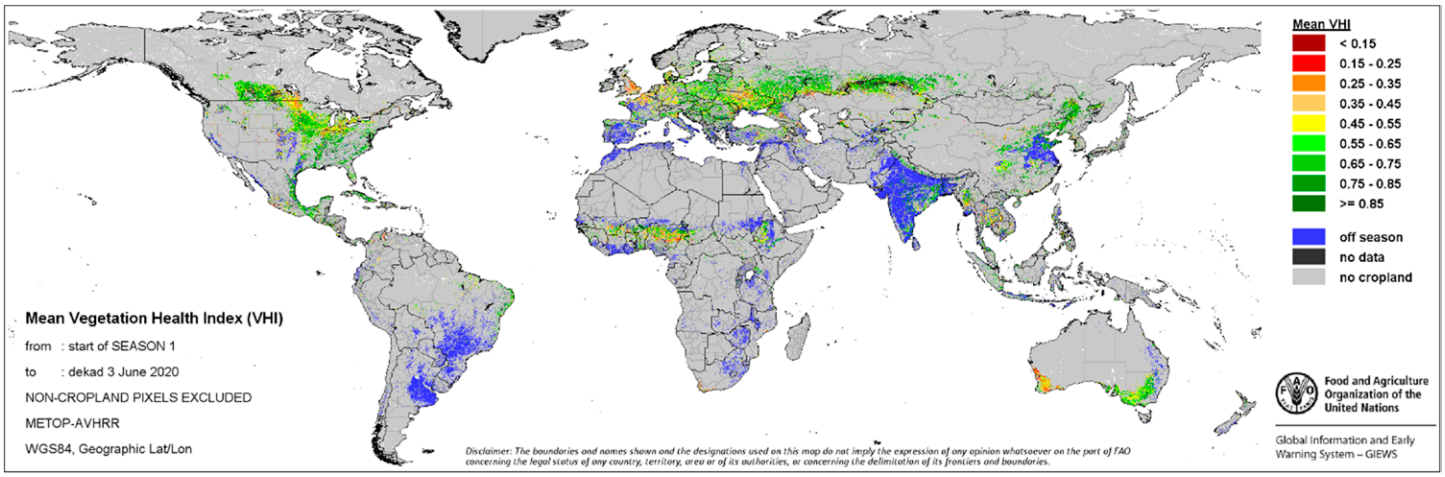

Fig. 5. Vegetation health index for croplands based on NDVI from AVHRR on MetOp (3 Jun 2020). Image from the Food and Agricultural Organization (www.fao.org/giews/earthobservation/asis/index_1.jsp?lang=en).

The Intergovernmental Panel on Climate Change (IPCC 2007) and the U.S. Climate Change Science Program (USCCSP; USCCSP 2004) used trends in biophysical variables based on AVHRR data in their assessments of climate change. Spectral and temporal measurements from AVHRR were used to create continental- and global-scale land-cover maps (Loveland et al. 2000), which eventually resulted in improved parameterization schemes in numerical weather prediction models. AVHRR-derived fraction of green vegetation provided a critical input to the land parameterization which greatly improved the performance of the NOAA numerical weather prediction models (Gutman and Ignatov 1998). Global land-cover maps from AVHRR produced under the guidance of the International Geosphere–Biosphere Program (Loveland et al. 2000) formed the basis of a wide range of environmental studies and are widely used by agencies such as the UN Environmental Program. Biomass burning has a huge impact on climate and human health and under international programs such as the IGBP and Global Observations of Forest and Land Cover Dynamics (GOFC/GOLD), several initiatives were started to routinely detect, map and monitor fires and biomass burning using AVHRR (Li et al. 2001). Using vegetation indices as a proxy indicator of rainfall, epidemiologists developed models that linked NDVI with the prevalence of arthropod vectors, such as ticks and mosquitoes, which led to a new discipline in using satellite data for spatially modeling and mapping patterns of occurrence of diseases such as malaria (Rogers et al. 2002).

AVHRR contributions to cloud studies

The AVHRR provided the first global surveys of cloudiness at a high spatial resolution from a single sensor with enough spectral information for a full suite of cloud properties, including cloud detection, phase, temperature, height, pressure, optical depth, particle size, and water path. The channels on the AVHRR were not chosen for cloud remote sensing beyond the initial requirement to detect clouds. For example, the split-window channels were included for sea surface temperature but proved useful in providing information on the vertical distribution (macrophysics) and the optical depth and particle size (microphysics) of cirrus clouds (Parol et al. 1991). Also, the pairing of band 3b (3.75 μm) with band 1 (0.65 μm) or band 2 (0.86 μm) has proven capable of extracting the cloud microphysical products of cloud optical depth and cloud particle size (Platnick and Valero 1995). The latest versions of the AVHRR switch to band 3a (1.6 μm) during daylight operations. Band 3a also allows for estimation of cloud microphysics, albeit within a spectral band that exhibits much less cloud particle absorption. These cloud retrieval methods led to the development at the operational space agencies of real-time retrieval systems such as the Clouds from AVHRR Extended (CLAVR-x) (Thomas et al. 2004), the NOAA polar product processing system and the AVHRR Processing Scheme Over Clouds, Land and Ocean (APOLLO) (Kriebel et al. 1994). These operational AVHRR products provided information on phenomena, such as aviation hazards and convective cloud monitoring, and have been used to verify output from numerical weather prediction. As the AVHRR record grew in length, global cloud climatologies were explored. While the AVHRR was not designed for climate work, its thermal calibration system has proven stable and accurate enough for cloud studies. The solar channels lack an onboard calibration system but various methods have been employed to make consistent and accurate solar reflectance observations (Heidinger et al. 2010).

Several projects have attempted to derive multidecadal cloud climatologies from AVHRR. The first was the International Satellite Cloud Climatology Project (ISCCP) (Rossow and Schiffer 1991), which used the AVHRR in the polar regions, and wherever the global geostationary sensors had gaps. ISCCP only used the 0.65- and 11-μm observations, whereas the follow-on algorithms used all the AVHRR bands. The NASA/NOAA Pathfinder Projects used the AVHRR sensor to develop and test concepts to be used on the NASA EOS Mission (2000–present)

(Maiden and Greco 1994). Pathfinder Atmospheres (PATMOS) was one such project, which generated cloud amount, aerosol optical depth, and some radiation budget parameters from the AVHRRs in afternoon orbits (Stowe et al. 2002). Its successor (PATMOS-x) (Heidinger et al. 2014) created a full suite of microphysical and macrophysical properties from all of the AVHRRs, and its data record continues. A cloud climatology specific to the polar regions was generated by the AVHRR Polar Pathfinder-Extended Project (APP-x) (Key et al. 2016). In addition, other AVHRR climatologies have begun in recent years including the Satellite Application Facility on Climate Monitoring (CM SAF) Clouds, Albedo and Radiation dataset from AVHRR data (CLARA) (Karlsson et al. 2013), the NASA Langley AVHRR Satellite Cloud and Radiation Property retrieval System (SatCORPS) climatology (Minnis et al. 2016), and the AVHRR cloud climatology from the ESA Climate Change Initiative (Cloud CCI) (Hollmann et al. 2013). These climate records have been used to document the growth in height of tropical clouds (Marvel et al. 2015), the expansion of the tropics (Norris et al. 2016) and the impact of the anthropogenic aerosol on cloud microphysical properties including precipitation (Bennartz et al. 2011). The global observations of AVHRR provide a means of monitoring global phenomena such as El Niño, which have dramatic impacts on the global distribution of cloudiness.

Figure 6 shows the ice cloud fraction from the PATMOS-x AVHRR dataset during four of the El Niño events in the AVHRR record. During El Niño conditions, the Walker circulation over the equator is disrupted (Wang 2002), characterized by moist air rising in the equatorial central and eastern Pacific, and descending over south east Asia disrupting the precipitation in these areas. All of these El Niño events occurred before NASA's Earth Observing System satellite data were available, and therefore AVHRR is the only global sensor to study them over extended periods of time. Knowledge of the response of cloudiness to shorter-term cycles like El Niño is important to characterize and better understand those processes. In addition, that knowledge can lead to a better understanding the sensitivity of cloudiness to climate change, which aids the understanding of multidecadal changes.

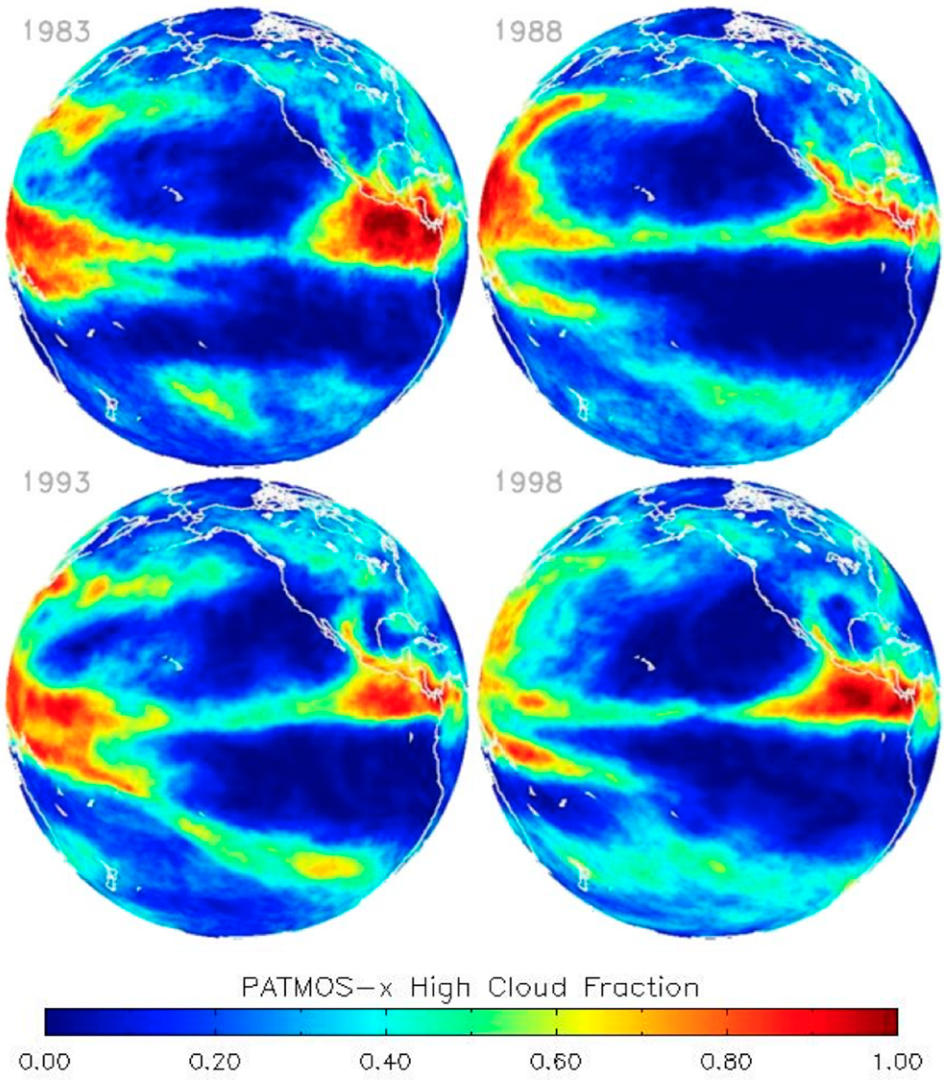

Fig. 6. Annual average of high-cloud fraction estimated from AVHRR measurements over the Pacific during four El Niño years.

AVHRR contributions to aerosol studies

Aerosol particles in the atmosphere absorb and scatter visible and near-IR radiation, and can thus be detected from satellite data. For surface remote sensing, aerosols are treated as an atmospheric hindrance that need to be detected and corrected for accurate measurement of land/ocean signals, whereas atmospheric scientists are interested in studying the aerosols themselves as they impact Earth's climate. In AVHRR reflectance bands 1 and 2, and newly added band 3A on AVHRR/3, ocean is close to a blackbody, so that the TOA reflectances are composed of two contributions: a well-characterized Rayleigh (molecular) scattering, which can be easily accounted for, and the unknown aerosol scattering. Following pioneering studies of Griggs (Griggs 1975), the first-ever operational aerosol product over global ocean from AVHRR band 1 was launched at NOAA in the late 1980s (Rao et al. 1989). The NOAA heritage algorithm retrieved column aerosol optical depth (AOD) using a single band, assuming that the aerosol type (microphysics, chemistry) remains unchanged over global ocean. This first-generation AOD product proved instrumental to study the global distribution of tropospheric aerosols, and to monitor the evolution (dispersion and circulation) of stratospheric aerosols, following two major volcanic eruptions in the late twentieth century: Mount Pinatubo in 1991 (Stowe et al. 1992) and retrospectively El Chichón in 1982 (Strong and Stowe 1993). In the two following decades, the NOAA operational algorithm underwent two upgrades, the second generation (Stowe et al. 1997) (which continued to employ only band 1) and the third generation (which added single-channel retrievals in bands 2 and 3A) (Ignatov et al. 2004a). The newer algorithms, however, continued to employ the same single-channel methodology, in which all parameters of the retrieval algorithm, except AOD, were set globally nonvariable, and various flavors of the NOAA single-channel algorithm were employed to generate long-term aerosol records using the PATMOS system (Stowe et al. 2002). To more accurately estimate AOD, the aerosol community explored estimating aerosol particle size from two AVHRR reflectance bands and also specifying the aerosol model used in the retrievals (Higurashi and Nakajima 1999; Mishchenko et al. 1999). However, estimating finer aerosol characteristics such as aerosol size distribution and/or type from AVHRR remains limited due to the number of reflectance bands and their lack of onboard calibration (Ignatov et al. 1998). Moreover, the impact of multichannel AVHRR methods of the retrieved AOD remains small for typical AOD values over oceans, and includes other sources of uncertainty (Laszlo et al. 2008). Nevertheless, several attempts were made to overcome this limitation and retrieve long-term particle size and improved AOD records from AVHRR (Geogdzhayev et al. 2004; Zhao et al. 2008) to detect trends in the derived aerosol characteristics (Mishchenko and Geogdzhayev 2007; Zhao et al. 2008). Improvements to intercalibrations among AVHRRs on different satellites have been instrumental to the construction of more consistent long-term global aerosol records from AVHRR (Zhao et al. 2008), and the identification of the regional and global impact of various phenomena, such as the transport of Saharan dust particles, smoke and biomass burning and volcanic eruptions (Fig. 7). Aerosol retrievals from AVHRR over land have been also studied (Kaufman and Sendra 1988; Holben et al. 1992; Hauser et al. 2005; Hsu et al. 2017), but to our knowledge did not result in any long-term reprocessed datasets, for use in climatological studies or long-term model analysis (Gelaro et al. 2017).

AVHRR contributions to polar region studies

Over the last two decades there have been dramatic changes in Arctic sea ice, surface temperature, snow cover, glaciers, and the ice sheets of Greenland and Antarctica. Changes in Arctic climate do not occur in isolation; there is strong evidence that they influence midlatitude weather (Cohen et al. 2014). Therefore, the importance of monitoring and evaluating changes in the polar regions has never been greater. With 14 overlapping orbits per day that provide robust coverage of the polar regions and a time series that began four decades ago, the AVHRR is well suited to observing and assessing changes in Arctic and Antarctic climates.

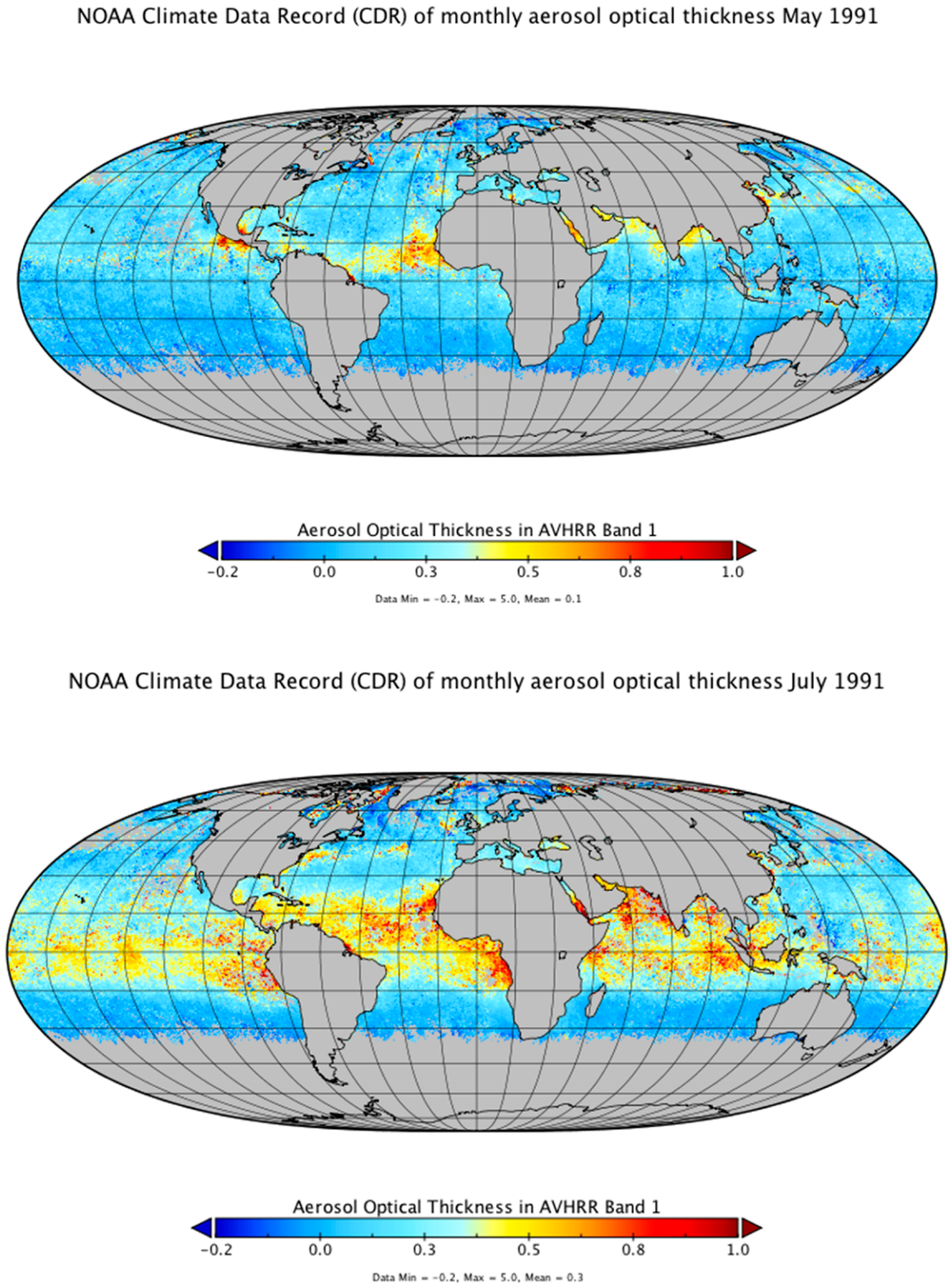

Fig. 7. Monthly mean aerosol optical thickness in AVHRR band 1 over the oceans during (top) May and (bottom) July 1991. Mount Pinatubo erupted on 15 Jun 1991 and the volcanic ash circled the globe in 21 days (Stowe et al. 1992). Data from National Center for Environmental Information (Zhao et al. 2017).

The most consistent, long-term, and comprehensive dataset available specifically for high-latitude studies is the AVHRR Polar Pathfinder (APP). APP is a fundamental climate data record (CDR) that provides channel reflectances and brightness temperatures over both polar regions as gridded, twice-daily local solar time composites from 1982

through the present. The APP-x is a thematic CDR built on APP that provides information on surface temperature, surface albedo, sea ice thickness, cloud properties, and surface and top-of-atmosphere radiative fluxes (Key et al. 2016). APP and APP-x were first developed in the 1990s (Maslanik et al. 1997; Meier et al. 1997). They have since been redesigned, improved, and enhanced. The two climate data records are distributed by the NOAA National Centers for Environmental Information (NCEI) (Key et al. 2019a,b).

One of the first climatological applications of APP-x yielded the discovery that, over the period 1982–99, the central Arctic Ocean had become cloudier and warmer in spring and summer but had become less cloudy and cooler in winter (Wang and Key 2003). The implication was that if seasonal cloud amounts had not changed the way they did, the Arctic would have warmed even more. Using APP-x in an Antarctic study, it was discovered that clouds over the Antarctic continent have a radiative warming effect on the surface for every month of the year. This is in sharp contrast to the effect of clouds globally, which is to cool the surface on average. APP-x has also been used to examine the snow-albedo feedback (Fernandes et al. 2009) and the importance of the ice-albedo feedback relative to the snow-albedo feedback (Letterly et al. 2018). Regarding the latter, it was determined that the positive (increasing) trend in the absorption of solar radiation at the Arctic Ocean surface due to sea ice decline is more than double that trend over Arctic land that result from reductions in snow cover. Furthermore, the magnitude of the ice-albedo feedback is 4 times larger than that of the snow-albedo feedback in summer. It appears, therefore, that decreasing sea ice cover has been the dominant radiative feedback for the last few decades, not changes in terrestrial snow cover. However, clouds also play an important role in a changing Arctic climate. On a regional scale, for example, trends in cloud cover derived from AVHRR data have been shown to have a significant influence on the surface radiation budget (Fig. 8). While we now have more robust satellite imagers such as VIIRS and MODIS, the time-tested AVHRR will continue to be a critical data source in polar climate studies for years to come.

The AVHRR has also been used for near-real-time analysis and monitoring of the high latitudes. AVHRR data are used to derive atmospheric winds (Velden et al. 2005;

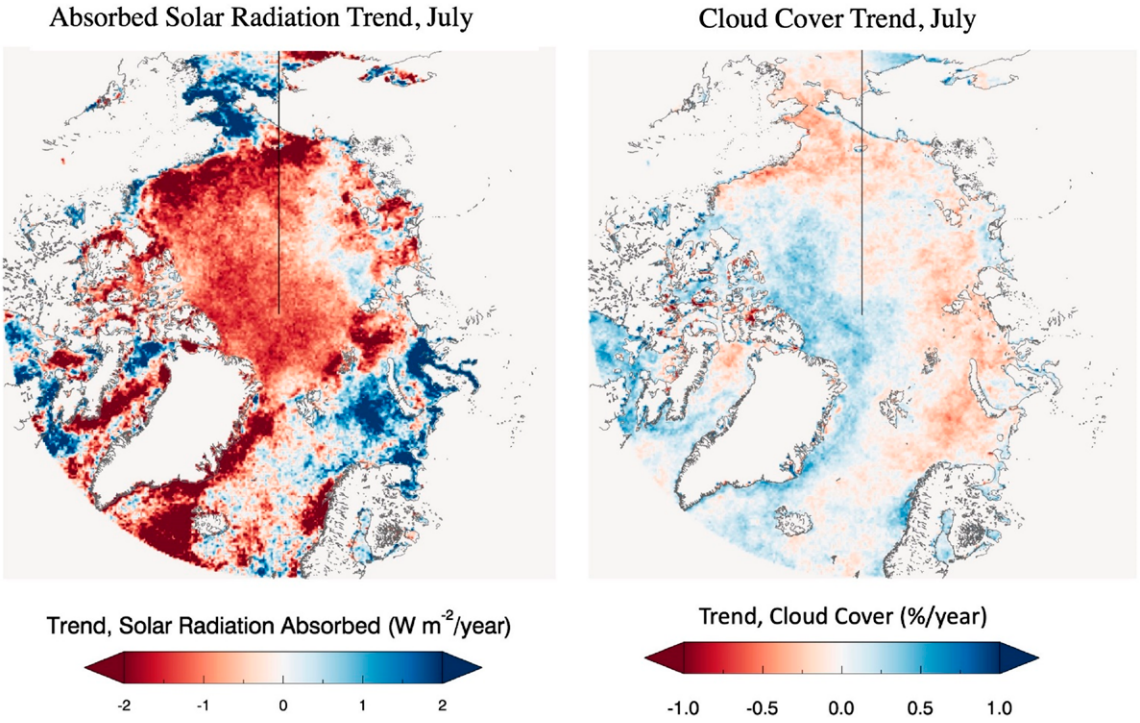

Fig. 8. Trends in (left) absorbed shortwave radiation and (right) cloud cover over the Arctic Ocean during July 1982–2015, from APP-x. The vertical line indicates 180° longitude from the North Pole.

Dworak and Key 2009), which are delivered to various NWP centers worldwide for assimilation in numerical models. For many years, AVHRR was also used for daily snow-cover monitoring (Simpson et al. 1998; Ramsay 1998; Romanov et al. 2000; Zhao and Fernandes 2009), sea ice cover (e.g., Burns et al. 1992), and sea ice surface temperature (Key and Haefliger 1992). Some of these applications continue today. Finally, APP-x is updated daily and can therefore be used to monitor recent changes in cloud properties, surface albedo, surface temperature, and sea ice thickness.

AVHRR contributions to oceanography

In the early 1980s, NOAA pioneered a global SST product from the second-generation AVHRR. SST measurements are routinely assimilated into numerical weather prediction models. The community consensus multichannel and nonlinear SST (MC/NLSST) algorithms employ split-window bands 4/5 (11/12 μm), often supplemented at night with the transparent band 3 (3.7 μm) (McClain et al. 1985). Reprocessing helps to reduce errors in the SST estimate caused by aerosols, unstable orbits and sensors, etc. It can also reduce variations associated with changes in the operational algorithm. However, there are still errors that need to be accounted for, as shown by Reynolds et al. (2007). For long climate-quality analyses some sort of bias adjustment is therefore needed. Typically, the bias adjustment is performed against in situ SST observations. This effectively gives an SST estimate of the in situ bulk measure depth, typically 0.2–1 m, by adjusting the AVHRR SST estimate, which physically only senses the sea surface skin temperature.

Three long-term SST reprocessing efforts have been undertaken, the NOAA/NASA Pathfinder program (Kilpatrick et al. 2001), the ESA Climate Change Initiative (Merchant et al. 2014), and the NOAA Reanalysis (RAN) (Ignatov et al. 2016), aimed at the derivation of a consistent long-term SST records from multiple AVHRR/2 and AVHRR/3 instruments flown on board numerous NOAA and MetOp satellites. To support Cal/Val of reprocessed AVHRR SST records, NOAA has also created a uniformly quality-controlled dataset of in situ SSTs, covering all satellite era from 1981 to the present (Xu and Ignatov 2014). The major limitations of AVHRR SST time series are unstable thermal calibration (He et al. 2016) and orbital characteristics of the NOAA satellites (Ignatov et al. 2004b). To mitigate those, some empirical corrections and/or stabilizations have been applied to the time series of derived SSTs (or input brightness temperatures in bands 3, 4, and 5). An important operational long-term SST analysis was developed by using an optimum interpolation technique (Reynolds et al. 2007) at 0.25°, where both day and night AVHRR SST estimates are bias adjusted to minimize large-scale biases relative to the available in situ data. This analysis gives consistent time series over the satellite period, and has proved to be important for climate studies (Fig. 9) and monitoring of long-term variations. The reprocessed SST records proved instrumental to create long-term reanalysis (Gelaro et al. 2017) and to support climate change studies. Nevertheless, the residual errors of those corrections remain large. Work is underway at NOAA to mitigate those, by generating a more stable and consistent AVHRR L1b record, and generating a more stable and consistent SST record from higher quality L1b radiances. Higher-resolution level 4 products, such as the NOAA Geo-Polar Blended analysis, are also being explored (Maturi et al. 2017).

Summary

AVHRR data from the past four decades constitute the longest continuous record of global remote sensing observations from a visible–infrared imager. These data have made enormous contributions to our understanding of ocean, land, atmosphere, and cryosphere processes, and their changes over time. Numerous applications and studies have evolved based on the observations from this instrument, including monitoring droughts, understanding the

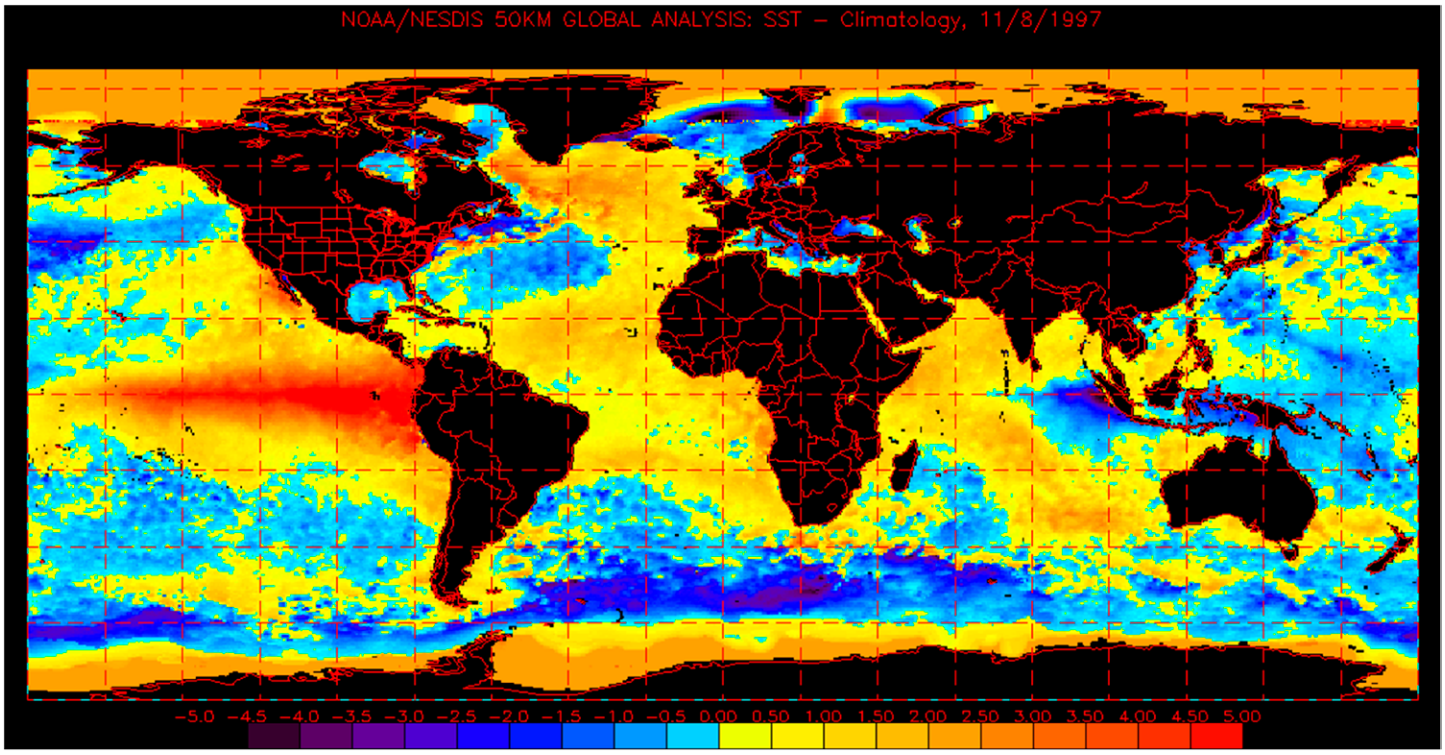

Fig. 9. AVHRR SST anomaly (deviation from climatology) along the equatorial Pacific on 8 Nov 1997 indicating El Niño–Southern Oscillation (NOAA Coral Reef Watch; https://coralreefwatch.noaa.gov/product/50km/).

global cloud climatology, warming of the Arctic and associated feedbacks, and changes in SST that have a global impact on weather patterns. AVHRR data have been reprocessed periodically for stability and consistency among sensors on different satellites. Observations from new, more capable, and better-calibrated sensors such as VIIRS and METImage will continue and extend the record of AVHRR products well into the future. Nevertheless, we will continue to rely on historic AVHRR data for retrospective studies to understand how our Earth is changing.

Acknowledgments. This research was supported by the NOAA Climate Data Records program and the Joint Polar Satellite System (JPSS) Program Office. We thank Xuanji Wang, Yinghui Liu, Aaron Letterly, and Rich Dworak for their contributions to the APP and APP-x products. We also thank Boris Petrenko and Victor Pryamitsyn for the contributions to AVHRR Reanalysis (RAN), and Kai He and Feng Xu for their help with the NOAA 3S and *i*Quam systems. The views, opinions, and findings contained in this report are those of the authors and should not be construed as an official National Oceanic and Atmospheric Administration or U.S. Government position, policy, or decision. AVHRR is manufactured by ITT Exelis (L3Harris). The authors thank the three anonymous reviewers for their valuable comments and inputs on the original manuscript.

References

Bennartz, R., J. Fan, J. Rausch, L. R. Leung, and A. K. Heidinger, 2011: Pollution from China increases cloud droplet number, suppresses rain over the East China Sea. *Geophys. Res. Lett.*, **38**, L09704, https://doi.org/10.1029/2011GL047235.

Brown, M. E., and E. B. Brickley, 2012: Evaluating the use of remote sensing data in the U.S. Agency for International Development Famine Early Warning Systems network. *J. Appl. Remote Sens.*, **6**, 063511, https://doi.org/10.1117/1.JRS.6.063511.

Burns, B. A., M. Schmidt-Grottrup, and T. Viehoff, 1992: Methods for digital analysis of AVHRR sea ice images. *IEEE Trans. Geosci. Remote Sens.*, **30**, 589–602, https://doi.org/10.1109/36.142937.

Cao, C., J. Sullivan, E. Maturi, and J. Sapper, 2004: The effect of orbit drift on the calibration of the 3.7 μm channel of the AVHRR onboard NOAA-14 and its impact on night-time sea surface temperature retrievals. *Int. J. Remote Sens.*, **25**, 975–986, https://doi.org/10.1080/0143116031000095899.

——, X. Xiong, A. Wu, and X. Wu, 2008: Assessing the consistency of AVHRR and MODIS L1B reflectance for generating fundamental climate date records. *J. Geophys. Res.*, **113**, D09114, https://doi.org/10.1029/2007JD009363.

——, F. J. D. Luccia, X. Xiong, R. Wolfe, and F. Weng, 2014: Early on-orbit performance of the visible infrared imaging radiometer suite onboard the Suomi National Polar-Orbiting Partnership (S-NPP) satellite. *IEEE Trans. Geosci. Remote Sens.*, **52**, 1142–1156, https://doi.org/10.1109/TGRS.2013.2247768.

Cohen, J., and Coauthors, 2014: Recent Arctic amplification and extreme mid-latitude weather. *Nature Geosci.*, **7**, 627–637, https://doi.org/10.1038/ngeo2234.

Cracknell, A. P., 1997: *The Advanced Very High Resolution Radiometer (AVHRR)*. Taylor and Francis, 534 pp.

Dworak, R., and J. Key, 2009: Twenty years of polar winds from AVHRR: Validation and comparison to the ERA-40. *J. Appl. Meteor. Climatol.*, **48**, 24–40, https://doi.org/10.1175/2008JAMC1863.1.

Fernandes, R., H. Zhao, X. Wang, J. Key, X. Qu, and A. Hall, 2009: Controls on Northern Hemisphere snow albedo feedback quantified using satellite Earth observations. *Geophys. Res. Lett.*, **36**, L21702, https://doi.org/10.1029/2009GL040057.

Gelaro, R., and Coauthors, 2017: The Modern-Era Retrospective Analysis for Research and Applications, version 2 (MERRA-2). *J. Climate*, **30**, 5419–5454, https://doi.org/10.1175/JCLI-D-16-0758.1.

Geogdzhayev, I. V., M. I. Mishchenko, L. Liu, and L. Remer, 2004: Global two-channel AVHRR aerosol climatology: Effects of stratospheric aerosols and preliminary comparisons with MODIS and MISR retrievals. *J. Quant. Spectrosc. Radiat. Transfer*, **88**, 47–59, https://doi.org/10.1016/j.jqsrt.2004.03.024.

Griggs, M., 1975: Measurements of atmospheric aerosol optical thickness over water using ERTS-1 data. *J. Air Pollut. Control Assoc.*, **25**, 622–626, https://doi.org/10.1080/00022470.1975.10470118.

Gutman, G., and A. Ignatov, 1998: The derivation of the green vegetation fraction from NOAA/AVHRR data for use in numerical weather prediction models. *Int. J. Remote Sens.*, **19**, 1533–1543, https://doi.org/10.1080/014311698215333.

Hauser, A., D. Oesch, N. Foppa, and S. Wunderle, 2005: NOAA AVHRR derived aerosol optical depth over land. *J. Geophys. Res.*, **110**, D08204, https://doi.org/10.1029/2004JD005439.

He, K., A. Ignatov, Y. Kihai, C. Cao, and J. Stroup, 2016: Sensor Stability for SST (3S): Toward improved long-term characterization of AVHRR thermal bands. *Remote Sens.*, **8**, 346, https://doi.org/10.3390/rs8040346.

Heidinger, A. K., C. Cao, and J. T. Sullivan, 2002: Using Moderate Resolution Imaging Spectrometer (MODIS) to calibrate advanced very high resolution radiometer reflectance channels. *J. Geophys. Res.*, **107**, 4702, https://doi.org/10.1029/2001JD002035.

——, W. C. Straka, C. C. Molling, J. T. Sullivan, and X. Wu, 2010: Deriving an inter-sensor consistent calibration for the AVHRR solar reflectance data record. *Int. J. Remote Sens.*, **31**, 6493–6517, https://doi.org/10.1080/01431161.2010.496472.

——, M. J. Foster, A. Walther, and X. Zhao, 2014: The Pathfinder Atmospheres–Extended AVHRR climate dataset. *Bull. Amer. Meteor. Soc.*, **95**, 909–922, https://doi.org/10.1175/BAMS-D-12-00246.1.

Higurashi, A., and T. Nakajima, 1999: Development of a two-channel aerosol retrieval algorithm on a global scale using NOAA AVHRR. *J. Atmos. Sci.*, **56**, 924–941, https://doi.org/10.1175/1520-0469(1999)056<0924:DOATCA>2.0.CO;2.

Holben, B. N., 1986: Characteristics of maximum-value composite images from temporal AVHRR data. *Int. J. Remote Sens.*, **7**, 1417–1434, https://doi.org/10.1080/01431168608948945.

——, E. Vermote, Y. J. Kaufman, D. Tanre, and V. Kalb, 1992: Aerosol retrieval over land from AVHRR data-application for atmospheric correction. *IEEE Trans. Geosci. Remote Sens.*, **30**, 212–222, https://doi.org/10.1109/36.134072.

Hollmann, R., and Coauthors, 2013: The ESA Climate Change Initiative: Satellite data records for essential climate variables. *Bull. Amer. Meteor. Soc.*, **94**, 1541–1552, https://doi.org/10.1175/BAMS-D-11-00254.1.

Hsu, N. C., J. Lee, A. M. Sayer, N. Carletta, S.-H. Chen, C. J. Tucker, B. N. Holben, and S.-C. Tsay, 2017: Retrieving near-global aerosol loading over land and ocean from AVHRR. *J. Geophys. Res. Atmos.*, **122**, 9968–9989, https://doi.org/10.1002/2017JD026932.

Hutchinson, C. F., 1991: Uses of satellite data for famine early warning in sub-Saharan Africa. *Int. J. Remote Sens.*, **12**, 1405–1421, https://doi.org/10.1080/01431169108929733.

Ignatov, A., L. Stowe, and R. Singh, 1998: Sensitivity study of the Ångström exponent derived from AVHRR over the oceans. *Adv. Space Res.*, **21**, 439–442, https://doi.org/10.1016/S0273-1177(97)00926-5.

——, J. Sapper, S. Cox, I. Laszlo, N. R. Nalli, and K. B. Kidwell, 2004a: Operational Aerosol Observations (AEROBS) from AVHRR/3 on board NOAA-KLM satellites. *J. Atmos. Oceanic Technol.*, **21**, 3–26, https://doi.org/10.1175/1520-0426(2004)021<0003:OAOAFO>2.0.CO;2.

——, I. Laszlo, E. D. Harrod, K. B. Kidwell, and G. P. Goodrum, 2004b: Equator crossing times for NOAA, ERS and EOS sun-synchronous satellites. *Int. J. Remote Sens.*, **25**, 5255–5266, https://doi.org/10.1080/01431160410001712981.

——, and Coauthors, 2016: AVHRR GAC SST reanalysis version 1 (RAN1). *Remote Sens.*, **8**, 315, https://doi.org/10.3390/rs8040315.

IPCC, 2007: *Climate Change 2007: The Physical Science Basis*. Cambridge University Press, 996 pp.

James, M. E., and S. N. V. Kalluri, 1994: The pathfinder AVHRR land data set—An improved coarse resolution data set for terrestrial monitoring. *Int. J. Remote Sens.*, **15**, 3347–3363, https://doi.org/10.1080/01431169408954335.

Justice, C. O., J. R. G. Townshend, B. N. Holben, and C. J. Tucker, 1985: Analysis of the phenology of global vegetation using meteorological satellite data. *Int. J. Remote Sens.*, **6**, 1271–1318, https://doi.org/10.1080/01431168508948281.

Kalluri, S., C. Cao, A. Heidinger, A. Ignatov, and J. Key, 2019: The last Advanced Very High Resolution Radiometer. *2019 IEEE Int. Geoscience and Remote Sensing Symp.*, Yokohama, Japan, IEEE, 8388–8391, https://doi.org/10.1109/IGARSS.2019.8897974.

Karlsson, K. G., and Coauthors, 2013: CLARA-A1: A cloud, albedo, and radiation dataset from 28 yr of global AVHRR data. *Atmos. Chem. Phys.*, **13**, 5351–5367, https://doi.org/10.5194/acp-13-5351-2013.

Kaufman, Y. J., and C. Sendra, 1988: Algorithm for automatic atmospheric corrections to visible and near-IR satellite imagery. *Int. J. Remote Sens.*, **9**, 1357–1381, https://doi.org/10.1080/01431168808954942.

Key, J., and M. Haefliger, 1992: Arctic ice surface temperature retrieval from AVHRR thermal channels. *J. Geophys. Res.*, **97**, 5885–5893, https://doi.org/10.1029/92JD00348.

——, X. J. Wang, Y. H. Liu, R. Dworak, and A. Letterly, 2016: The AVHRR Polar Pathfinder climate data records. *Remote Sens.*, **8**, 167, https://doi.org/10.3390/rs8030167.

——, Y. Liu, and X. Wang, 2019a, National Center for Environmental Information: NOAA Climate Data Record of AVHRR Polar Pathfinder Extended (APP-X),

version 2, NOAA NCEI, accessed 18 January 2021, https://doi.org/10.25921/AE96-0E57.

_____, Y. Liu, and X. Wang, 2019b, National Center for Environmental Information: NOAA Climate Data Record of AVHRR Polar Pathfinder (APP), version 2, NOAA NCEI, accessed 18 January 2021, https://doi.org/10.25921/X2X1-JR34.

Kidwell, K. B., 1995: NOAA Polar Orbiter data (TIROS-N, NOAA-6, NOAA-7, NOAA-8, NOAA-9, NOAA-10, NOAA-11, NOAA-12, and NOAA-14) users guide. NOAA/NESDIS Rep., 410 pp.

Kilpatrick, K. A., G. P. Podestá, and R. Evans, 2001: Overview of the NOAA/NASA Advanced Very High Resolution Radiometer Pathfinder algorithm for sea surface temperature and associated matchup database. *J. Geophys. Res.*, **106**, 9179–9197, https://doi.org/10.1029/1999JC000065.

Kogan, F. N., 1997: Global drought watch from space. *Bull. Amer. Meteor. Soc.*, **78**, 621–636, https://doi.org/10.1175/1520-0477(1997)078<0621:GDWFS>2.0.CO;2.

Kriebel, K., G. Gesell, M. Kaestner, and H. Mannstein, 1994: Cloud detection in AVHRR and ATSR data with APOLLO. *Proc. SPIE*, **2309**, https://doi.org/10.1117/12.196703.

Laszlo, I., H. Liu, and A. Ignatov, 2008: Comparison of single-channel and multichannel aerosol optical depths derived from MAPSS data. *J. Geophys. Res.*, **113**, D19S90, https://doi.org/10.1029/2007JD009664.

Letterly, A., J. Key, and Y. H. Liu, 2018: Arctic climate: Changes in sea ice extent outweigh changes in snow cover. *Cryosphere*, **12**, 3373–3382, https://doi.org/10.5194/tc-12-3373-2018.

Li, Z., Y. J. Kaufamn, C. Ichoku, R. Fraser, A. Trishchenko, L. Giglio, J.-Z. Jin, and X. Yu, 2001: A review of AVHRR-based active fire detection algorithms: Principles, limitations and recommendations. *Global and Regional Vegetation Fire Monitoring from Space: Planning a Coordinated International Effort*, F. J. Ahren, J. G. Goldammer, and C. O. Justice, Eds., SPB Academic Publishing, 199–225.

Loveland, T. R., B. C. Reed, J. F. Brown, D. O. Ohlen, Z. Zhu, L. Yang, and J. W. Merchant, 2000: Development of a global land cover characteristics database and IGBP Discover from 1 km AVHRR data. *Int. J. Remote Sens.*, **21**, 1303–1330, https://doi.org/10.1080/014311600210191.

Maiden, M. E., and S. Greco, 1994: NASA's Pathfinder data set programme: Land surface parameters. *Int. J. Remote Sens.*, **15**, 3333–3345, https://doi.org/10.1080/01431169408954334.

Marvel, K., M. Zelinka, S. A. Klein, C. Bonfils, P. Caldwell, C. Doutriaux, B. D. Santer, and K. E. Taylor, 2015: External influences on modeled and observed cloud trends. *J. Climate*, **28**, 4820–4840, https://doi.org/10.1175/JCLI-D-14-00734.1.

Maslanik, J., C. Fowler, J. Key, T. Scambos, T. Hutchinson, and W. Emery, 1997: AVHRR-based Polar Pathfinder products for modeling applications. *Ann. Glaciol.*, **25**, 388–392, https://doi.org/10.3189/S0260305500014336.

Maturi, E., A. Harris, J. Mittaz, J. Sapper, G. Wick, X. Zhu, P. Dash, and P. Koner, 2017: A new high-resolution sea surface temperature blended analysis. *Bull. Amer. Meteor. Soc.*, **98**, 1015–1026, https://doi.org/10.1175/BAMS-D-15-00002.1.

McClain, E. P., W. G. Pichel, and C. C. Walton, 1985: Comparative performance of AVHRR-based multichannel sea surface temperatures. *J. Geophys. Res.*, **90**, 11 587–11 601, https://doi.org/10.1029/JC090iC06p11587.

Meier, W. N., J. A. Maslanik, C. W. Fowler, and J. R. Key, 1997: Multiparameter AVHRR-derived products for Arctic climate studies. *Earth Interact.*, **1**, https://doi.org/10.1175/1087-3562(1997)001<0001:MADPFA>2.3.CO;2.

Merchant, C. J., and Coauthors, 2014: Sea surface temperature datasets for climate applications from phase 1 of the European Space Agency Climate Change Initiative (SST CCI). *Geosci. Data J.*, **1**, 179–191, https://doi.org/10.1002/gdj3.20.

Minnis, P., K. Bedka, Q. Trepte, C. R. Yost, S. T. Bedka, B. Scarino, K. Khlopenkov, and M. M. Khaiyer, 2016: A consistent long-term cloud and clear-sky radiation property dataset from the Advanced Very High Resolution Radiometer (AVHRR). Climate Algorithm Theoretical Basis Doc., revision, 159 pp., https://doi.org/10.789/V5HT2M8T.

Mishchenko, M. I., and I. V. Geogdzhayev, 2007: Satellite remote sensing reveals regional tropospheric aerosol trends. *Opt. Express*, **15**, 7423–7438, https://doi.org/10.1364/OE.15.007423.

——, ——, B. Cairns, W. B. Rossow, and A. A. Lacis, 1999: Aerosol retrievals over the ocean by use of channels 1 and 2 AVHRR data: Sensitivity analysis and preliminary results. *Appl. Opt.*, **38**, 7325–7341, https://doi.org/10.1364/AO.38.007325.

NOAA, 2020: CoastWatch East Coast node. Accessed 12 August 2020, https://eastcoast.coastwatch.noaa.gov/index.php.

Norris, J. R., R. J. Allen, A. T. Evan, M. D. Zelinka, C. W. O'Dell, and S. A. Klein, 2016: Evidence for climate change in the satellite cloud record. *Nature*, **536**, 72–75, https://doi.org/10.1038/nature18273.

Parol, F., J. C. Buriez, G. Brogniez, and Y. Fouquart, 1991: Information content of AVHRR channels 4 and 5 with respect to the effective radius of cirrus cloud particles. *J. Appl. Meteor.*, **30**, 973–984, https://doi.org/10.1175/1520-0450-30.7.973.

Phillips, P., R. Bonsignori, P. Schlüssel, F. Schmülling, L. Spezzi, P. Watts, and I. Zerfowski, 2016: Overview of calibration and validation activities for the EUMETSAT polar system: Second generation (EPS-SG) visible/infrared imager (METimage). *Proc. SPIE*, **10000**, https://doi.org/10.1117/12.2240938.

Platnick, S., and F. P. J. Valero, 1995: A validation of a satellite cloud retrieval during ASTEX. *J. Atmos. Sci.*, **52**, 2985–3001, https://doi.org/10.1175/1520-0469(1995)052<2985:AVOASC>2.0.CO;2.

Ramsay, B., 1998: The interactive multisensor snow and ice mapping system. *Hydrol. Processes*, **12**, 1537–1546, https://doi.org/10.1002/(SICI)1099-1085(199808/09)12:10/11<1537::AID-HYP679>3.0.CO;2-A.

Rao, C. R. N., and J. Chen, 1999: Revised post-launch calibration of the visible and near-infrared channels of the Advanced Very High Resolution Radiometer (AVHRR) on the NOAA-14 spacecraft. *Int. J. Remote Sens.*, **20**, 3485–3491, https://doi.org/10.1080/014311699211147.

——, L. L. Stowe, and E. P. McClain, 1989: Remote sensing of aerosols over the oceans using AVHRR data: Theory, practice and applications. *Int. J. Remote Sens.*, **10**, 743–749, https://doi.org/10.1080/01431168908903915.

Reynolds, R. W., T. M. Smith, C. Liu, D. B. Chelton, K. S. Casey, and M. G. Schlax, 2007: Daily high-resolution-blended analyses for sea surface temperature. *J. Climate*, **20**, 5473–5496, https://doi.org/10.1175/2007JCLI1824.1.

Rogers, D. J., S. E. Randolph, R. W. Snow, and S. I. Hay, 2002: Satellite imagery in the study and forecast of malaria. *Nature*, **415**, 710–715, https://doi.org/10.1038/415710a.

Romanov, P., G. Gutman, and I. Csiszar, 2000: Automated monitoring of snow over North America with multispectral satellite data. *J. Appl. Meteor.*, **39**, 1866–1880, https://doi.org/10.1175/1520-0450(2000)039<1866:AMOSCO>2.0.CO;2.

Rossow, W. B., and R. A. Schiffer, 1991: ISCCP cloud data products. *Bull. Amer. Meteor. Soc.*, **72**, 2–20, https://doi.org/10.1175/1520-0477(1991)072<0002:ICDP>2.0.CO;2.

Salomonson, V. V., W. L. Barnes, P. W. Maymon, H. E. Montgomery, and H. Ostrow, 1989: MODIS: Advanced facility instrument for studies of the Earth as a system. *IEEE Trans. Geosci. Remote Sens.*, **27**, 145–153, https://doi.org/10.1109/36.20292.

Schneider, S. R., D. F. McGinnis, and J. A. Gatlin, 1981: Use of NOAA/AVHRR visible and near-infrared data for land remote sensing. NOAA Tech. Rep. NESS 84, 48 pp.

Simpson, J. J., J. R. Stitt, and M. Sienko, 1998: Improved estimates of the areal extent of snow cover from AVHRR data. *J. Hydrol.*, **204**, 1–23, https://doi.org/10.1016/S0022-1694(97)00087-5.

Stowe, L. L., R. M. Carey, and P. P. Pellegrino, 1992: Monitoring the Mt. Pinatubo aerosol layer with NOAA/11 AVHRR data. *Geophys. Res. Lett.*, **19**, 159–162, https://doi.org/10.1029/91GL02958.

——, A. M. Ignatov, and R. R. Singh, 1997: Development, validation, and potential enhancements to the second-generation operational aerosol product at the National Environmental Satellite, Data, and Information Service of the National Oceanic And Atmospheric Administration. *J. Geophys. Res.*, **102**, 16 923–16 934, https://doi.org/10.1029/96JD02132.

——, H. Jacobowitz, G. Ohring, K. R. Knapp, and N. R. Nalli, 2002: The Advanced Very High Resolution Radiometer (AVHRR) Pathfinder Atmosphere (PATMOS) climate dataset: Initial analyses and evaluations. *J. Climate*, **15**, 1243–1260, https://doi.org/10.1175/1520-0442(2002)015<1243:TAVHRR>2.0.CO;2.

Strong, A. E., and L. L. Stowe, 1993: Comparing stratospheric aerosols from El Chichón and Mount Pinatubo using AVHRR data. *Geophys. Res. Lett.*, **20**, 1183–1186, https://doi.org/10.1029/93GL01519.

Thomas, S. M., A. K. Heidinger, and M. J. Pavolonis, 2004: Comparison of NOAA's operational AVHRR-derived cloud amount to other satellite-derived cloud climatologies. *J. Climate*, **17**, 4805–4822, https://doi.org/10.1175/JCLI-3242.1.

Townshend, J. R. G., 1994: Global data sets for land applications from the Advanced Very High Resolution Radiometer: An introduction. *Int. J. Remote Sens.*, **15**, 3319–3332, https://doi.org/10.1080/01431169408954333.

Trishchenko, A. P., 2009: Effects of spectral response function on surface reflectance and NDVI measured with moderate resolution satellite sensors: Extension to AVHRR NOAA-17, 18 and MetOp-A. *Remote Sens. Environ.*, **113**, 335–341, https://doi.org/10.1016/j.rse.2008.10.002.

Tucker, C. J., and P. J. Sellers, 1986: Satellite remote-sensing of primary production. *Int. J. Remote Sens.*, **7**, 1395–1416, https://doi.org/10.1080/01431168608948944.

USCCSP, 2004: Our changing planet: The U.S. Climate Change Science Program for fiscal years 2004 and 2005: A report. USCCSP Rep., 159 pp.

Van Hoolst, R., H. Eerens, D. Haesen, A. Royer, L. Bydekerke, O. Rojas, Y. Li, and P. Racionzer, 2016: FAO's AVHRR-based Agricultural Stress Index System (ASIS) for global drought monitoring. *Int. J. Remote Sens.*, **37**, 418–439, https://doi.org/10.1080/01431161.2015.1126378.

Velden, C., and Coauthors, 2005: Recent innovations in deriving tropospheric winds from meteorological satellites. *Bull. Amer. Meteor. Soc.*, **86**, 205–224, https://doi.org/10.1175/BAMS-86-2-205.

Wang, C., 2002: Atmospheric circulation cells associated with the El Niño–Southern Oscillation. *J. Climate*, **15**, 399–419, https://doi.org/10.1175/1520-0442(2002)015<0399:ACCAWT>2.0.CO;2.

Wang, L. K., and C. Y. Cao, 2008: On-orbit calibration assessment of AVHRR longwave channels on MetOp-A using IASI. *IEEE Trans. Geosci. Remote Sens.*, **46**, 4005–4013, https://doi.org/10.1109/TGRS.2008.2001062.

Wang, X. J., and J. R. Key, 2003: Recent trends in Arctic surface, cloud, and radiation properties from space. *Science*, **299**, 1725–1728, https://doi.org/10.1126/science.1078065.

Xu, F., and A. Ignatov, 2014: In situ SST quality monitor (iQuam). *J. Atmos. Oceanic Technol.*, **31**, 164–180, https://doi.org/10.1175/JTECH-D-13-00121.1.

Zhang, X., L. Liu, and D. Yan, 2017: Comparisons of global land surface seasonality and phenology derived from AVHRR, MODIS, and VIIRS data. *J. Geophys. Res. Biogeosci.*, **122**, 1506–1525, https://doi.org/10.1002/2017JG003811.

Zhao, H., and R. Fernandes, 2009: Daily snow cover estimation from Advanced Very High Resolution Radiometer Polar Pathfinder data over Northern Hemisphere land surfaces during 1982–2004. *J. Geophys. Res.*, **114**, D05113, https://doi.org/10.1029/2008JD011272.

Zhao, T. X. P., I. Laszlo, W. Guo, A. Heidinger, C. Cao, A. Jelenak, D. Tarpley, and J. Sullivan, 2008: Study of long-term trend in aerosol optical thickness observed from operational AVHRR satellite instrument. *J. Geophys. Res.*, **113**, D07201, https://doi.org/10.1029/2007JD009061.

Zhao, X., and Coauthors, 2017: NOAA Climate Data Record (CDR) of AVHRR daily and monthly aerosol optical thickness (AOT) over global oceans, version 3. NOAA NCEI, accessed 18 January 2021, https://doi.org/10.7289/V5BZ642P.